applied sciences

MDPI

Article

Iridescent Techniques in Ceramics: Physico-Chemical Analysis and Colorimetric Characterization of the Headquarters of the Botín Foundation in Santander

Víctor Echarri-Iribarren [1,*], Ángel B. González-Avilés [1] and Valentín Viqueira-Pérez [2]

[1] Department of Building Construction, University of Alicante, 03690 San Vicente, Spain; angelb@ua.es
[2] Department of Optical Sciences, University of Alicante, 03690 San Vicente, Spain; valentin.viqueira@ua.es
* Correspondence: Victor.Echarri@ua.es; Tel.: +34-965-903677

Received: 5 February 2019; Accepted: 29 March 2019; Published: 12 April 2019

Featured Application: The iridescent effect of ceramic provides excellent visual and perceptual characteristics, being able to control the chromatic ranges produced in the function of diverse layers of enamel. It also provides a harmonious integration into environments of great landscape value when applied to building façades.

Abstract: In recent years, the use of porcelain stoneware in building envelopes has opened new lines of research and innovation favoring energy efficiency and the reduction of environmental impacts. However, there has been little research on its relationship with light vibration and reflectivity, visual perception, and integration in the urban environment and landscape. In this study, an analysis was conducted on the production and application of crafted pieces of porcelain stoneware, shaped in spherical caps, at the headquarters of the Botín Foundation in Santander (Spain). Various enamels with an iridescent-nacreous finish and metallic reflection were applied to the stoneware to generate a vibrant skin that would constantly change with natural light and the environment. A vitrification and metal deposition process were designed through successive applications of enamels and firings. The physico-chemical properties of the enameling and the microcracking factors that produced the iridescent effect were characterized. A colorimetric characterization was performed evaluating the goniochromatic or iridescent colors, measuring the spectral radiance factor of the light, and comparing these results with other ceramic pieces.

Keywords: ceramic; porcelain stoneware; iridescent-pearl; metal deposition; reflectance; goniochromatic colors; zirconium

1. Introduction

In recent decades, the ceramic industry has succeeded in renewing itself by transforming all its manufacturing processes and recovering the sector's characteristic innovative and technological nature. A renewal of this kind had not taken place since the end of the 19th century. Following a period in which glazed ceramic was confined to bathrooms and kitchens, glazed ceramic and porcelain stoneware are now being applied to most architectural elements, especially in façade claddings [1]. This recovery has fostered greater competitiveness and further development of constructive solutions capable of adapting ceramic materials to architecture's new functional, aesthetic, and economic needs [2]. A true ceramic revolution has been unfolding over the last 15 years thanks to big investments in manufacturing processes and ongoing research in new product designs. A new alliance between architecture and industry has generated a fresh potential for creative, artistic, and project developments. It would be fair to say that artisanship traditions left behind since modernist architecture have been recovered [3,4].

Architects used to design handcrafted ceramic tiles, made with traditional purpose-built materials and systems; this is now happening today, supported by all the technological advances, applied both to materials and the computerization of the manufacturing, decoration, and molding processes.

Ceramic has established itself as a versatile material [5] to which a wide range of coatings can be applied thanks to research both in the fabrication and post-fabrication processes. When observing the evolution of the industrial process, the turning point can be defined as the leading role of firing systems, the production revolution consisting of including single-deck kilns and the arrival of natural gas in the industry (1980–1993) [6]. Over this same period, innovations have taken place regarding the processes of clay wet grinding and atomization; the third-firing ancillary industry has emerged; new means of printing [7], cutting, etc. have been incorporated into the process. The inclusion of these new processes, and the huge levels of competitiveness reached over the 1994–2004 decade, have established the necessary foundations for mastering techniques to serve projects, laying techniques have notably improved and, linked to this research, new glazing techniques and surface treatments have been generated [8]. This new generation of ceramic materials is manifest in major, world-renowned architectural works: the Santa Caterina Market in Barcelona (Enric Miralles and Benedetta Tagliabue), the Spanish pavilion at the Aichi Expo (Alejandro Zaera and Farshid Moussavi), Les Logements Sociaux de Paris and the Saint Giles Central Court in London (Renzo Piano), or the Zaragoza Expo's pavilion (Patxi Mangado).

This study focuses on the iridescent effect of the ceramic tiles of the Fundación Botín building enclosure in Santander (Spain), designed by the architect Renzo Piano and completed in 2017. One of its circular ceramic tiles, 156 mm in diameter, was analyzed using X-ray diffraction (XRD) and scanning electron microscopy techniques. Glazes applied to the interior and exterior cladding were characterized based on a metal vitrification and deposition process; the physical-chemical properties and the microcracking factors that produce iridescent effects when reflecting sunlight were also determined. Finally, a colorimetric characterization of the tiles' glaze finishings was performed, the goniochromatic or iridescent colors were evaluated, and the light's spectral radiance factor was measured. Lastly, the results obtained were compared with other ceramic tiles.

2. Iridescent and Pearl Ceramic Techniques

The coating of ceramic supporting surfaces allows tiles to offer greatly diversified technical characteristics [9], in addition to a wide range of decoration options, leading to a range of highly differentiated and diversified products [10]. The ceramic tile or slab's final appearance usually results from crystallization process phases that confer different finishes: shine, opacity, biodegradation through oxidation, anti-slip, roughness, luster [11], reflectance [12], etc. Other possible phenomena are of an optical nature, due to the interaction of sunlight or artificial light with the materials [12]. Though these techniques are widely used in the paint, automotive, plastic, textile, and composite industries [13], etc., they need to be further developed in the ceramic sector [14].

There is a broad body of research into ceramic coatings, which encompasses functional and decorative aspects. The aim, on the one hand, is to achieve the maximum durability and resistance of enamel [15], non-slip properties, reduction of heating and thermal transmittance towards the interior of buildings, through their behavior when in contact with solar radiation [16], etc. As for the decorative aspects, extensive research has been conducted into pigments that improve reflection of artificial light in interior design, golden glow effects in other cases, metallic shine effects, less polluting solar reflectance in the public space [17], phosphorescent effect [18], and a whole host of other applications. Much of the research conducted to date is aimed at finding stable color pigments, such as yellow [19] or blue [20], sometimes using encapsulation techniques [21], the application of nanopigments [22], microemulsions or inkjet printing [23]. Zirconium oxide [24,25] and titanium oxide are widely used. The former offers very good qualities in terms of hardness, durability and stability in the form of zirconium silicate C@$ZrSiO_4$ [26,27].

A ceramic finishing effect produced since ancient times is the multicolored or iridescent effect. Iridescence constitutes one of the most beautiful optical phenomena. It can be found in some minerals and is characterized as the property of certain surfaces according to which light tones vary depending on the angle of observation of the surface. This optical phenomenon is not due to the materials' chemical composition or crystal structure but to the interaction of light with certain inclusions or structural defects in the materials.

This physical-optical phenomenon was produced as early as in the Bronze Age, by dispersing gold, silver or copper metal nanoparticles on an optically clear matrix [28]. In Iraq, they were used in lusterware, which consisted of a thin metallic film containing silver, copper, iron oxide, and cinnabar, applied within a reducing atmosphere on a glazed ceramic surface, producing beautiful iridescent reflections in different colors such as gold and ruby red [29]. Later, in the late Roman and Byzantine periods (2nd to 8th centuries AD), brownish incrustations were made of minerals such as opal, quartz, clay minerals, plagioclase, and calcite, generating an iridescent surface that was in contact with bulk pristine glass, as analyzed by G. Barbera and colleagues [30]. New materials and techniques were used In the European and Asian Middle Ages. Some glazes were covered by iridescent layers consisting of lead carbonate and phosphates due to glaze alterations. I. Garofano et al. succeeded in detailing the microstructure and composition of the final surface layers that produce the luster effect observed in some ceramic samples from the Alcazar of Seville, using PIXE and Rutherford backscattering spectrometry (RBS) [31]. Other studies have focused on the analysis of luster, a decoration effect consisting of a surface layer of silver and copper metal nanoparticles, a few hundred nanometers thick, incorporated into the glaze [32,33]. A colorful and iridescent metallic aspect is achieved taking advantage of the confined quantum optical response of metallic nanoparticles [34]. Today, similar techniques continue to be applied by depositing metals in different glazing layers, with singular examples such as the auditorium of La Algueña (Spain), winner of the ASCER prize in 2012, or the building analyzed in this study, the headquarters of the Botín Foundation in Santander.

The phenomenon of iridescence found in ceramic coatings can be due to several causes. The first is the dispersion of light [35] causing white light to decompose into its different colors when passing through a prism, with light refraction depending on the nature of the medium it travels through. Second, it can be produced by constructive and destructive interferences that occur in semi-transparent or multilayer structures when the reflected light interacts with the structure's different layers [12]. Finally, iridescence can be caused by the diffraction of light. This physical-optical phenomenon is mainly caused by the irregularities that light encounters in its trajectory, such as cavities of a similar size to the wavelength of the light that is diffracted. White light passes through these small spaces, pores or microcracks, or passes through thin layers of material with a varying refractive index that act as a prism, inducing the split of white light into all the colors of the spectrum. The wavelengths interfere with each other causing iridescence.

Numerous patents have been developed to produce these types of effects [36]. Various techniques and depositions of metals such as titanium [37], gold, silver, aluminum, zirconium [26,38,39] are used. The substrates are also subject to various geometries and compositions, such as transparent films, organic adhesives, glass spheres, metal resins, etc. [40].

Other iridescence treatments include pearlescence and the use of pearl pigments [41,42]. Anatase (TiO_2) pearl pigments are typically used [43], and applied to the ceramic substrate, followed by a calcination process. The substrates that TiO_2 is applied to are natural mica (muscovite), synthetic mica (fluoroflogopite) or a-alumina flakes [44]. In other cases, this process is carried out by coating mica flakes with a thin layer of TiO_2. To do this, a chemical bath deposition method is used where a homogeneous hydrolysis of $TiCl_4$ solutions is carried out in a highly acidic environment ($pH < 2$). Sometimes the effects produced have gold and silver reflections [45]. A variant is the use of thin nanocrystalline films of Ta_2O_5 and ZrO_2 on SiO_2 flakes, using a liquid synthesis [46]. The CeO_2 cerium oxide deposition application techniques are also satisfactory to achieve pearl effects with a special brightness, as well as iridescent effects [47]. When combined with other metals, a softer pearl effect

can be produced [48]. Finally, other techniques produce similar effects to those described, though with differences and nuances that place them in other categories of ceramic finishes, such as the use of titanium and cobalt (TiO_2@$CoAl_2O_4$) [49] for bright colors [50], zirconium pigments encapsulated with deep black colors [51], or iridescent metal effect surfaces based on zinc oxide (ZnO) [52].

3. Botín Foundation Headquarters in Santander. Ceramic and Light Reflection

The Botín Center is a cultural facility dedicated to artistic exhibitions and research located in the city of Santander (Cantabria, Spain) and dependent on the Botín Foundation (Figure 1). The project was promoted by the Botín Foundation, a private foundation created in 1964 by Marcelino Botín Sanz de Sautuola and his wife, María del Carmen Yllera Camino. This unique architectural work, inaugurated on 23 June 2017, is composed of two different sized sections supported on columns and partially suspended over the sea. The work is by the Italian architect Renzo Piano, winner of the Pritzker Prize in 1998. A structure of spaces and walkways, acting as a main hallway, link the two sections. The west section is dedicated to art, with a 2500 m^2 exhibition hall. A shopping and restaurant area is installed in the glazed basements. The east section is smaller and is dedicated to educational activities, with a large terrace overlooking the Bay of Santander and a 950 m^2 covered plaza on the ground floor.

Figure 1. View of the Botín Foundation headquarters in Santander. Photograph: Ángel de los Ríos. https://support.google.com/legal/answer/3463239?sa=X&ved=2ahUKEwir__2px4ngAhUuz4UKHSnND9AQlZ0DegQIARAB.

Luminosity and lightness, one of its essential design features, stand out. The construction is supported by pillars and columns forming a cantilever over the Bay of Santander and the old Albareda and Maura docks. The building also respects the height of the Pereda Gardens treetops. Light is reflected in the ceramic façade, composed of 280,000 discoidal and pearl tiles, adapted to the building's geometry, with an iridescent effect applied to the finishing layers.

The Botín Center's enclosure or cladding is solved by placing the following elements on the general steel structure: a system of sandwich panels with steel sheeting on the inside—the thermal insulation core, polyamide clips to join the sandwich system and an outer layer of aluminum profiled sheets clamped together (Figure 2). The latter guarantee watertightness while the Botín Art Center (CAB) Matting System, specifically developed for the building by the Disset company, is placed on top (Figure 3). The elements making up this latter system are as follow:

- Anodized aluminum clamps: mechanical fixing and leveling system.
- Metallic substructure of anodized aluminum profiles which are rectangular-shaped in the straight sections and circular-shaped in the curved sections.

- Continuous lining of aluminum ribbed sheets, produced by extrusion, with a seaside marine environment coating, mechanized using a thermal-friction system based on computer-aided design and computer aided manufacturing (CAD-CAM) system parameters, designed and programmed by Disset for this enclosure.
- Circular ceramic tiles, 156 mm in diameter, produced by Cumella Ceramics, mechanized using an aluminum anchor threaded into the aluminum sheets by means of a drill system with a suction cup and a calibrated tightening torque.
- Special aluminum tiles with a seaside coating for expansion joints, deck registers, evacuation as well as rainwater collection channels and roof anchors.
- Profiled aluminum sheet finishing with seaside coating, around the enclosure's perimeter.

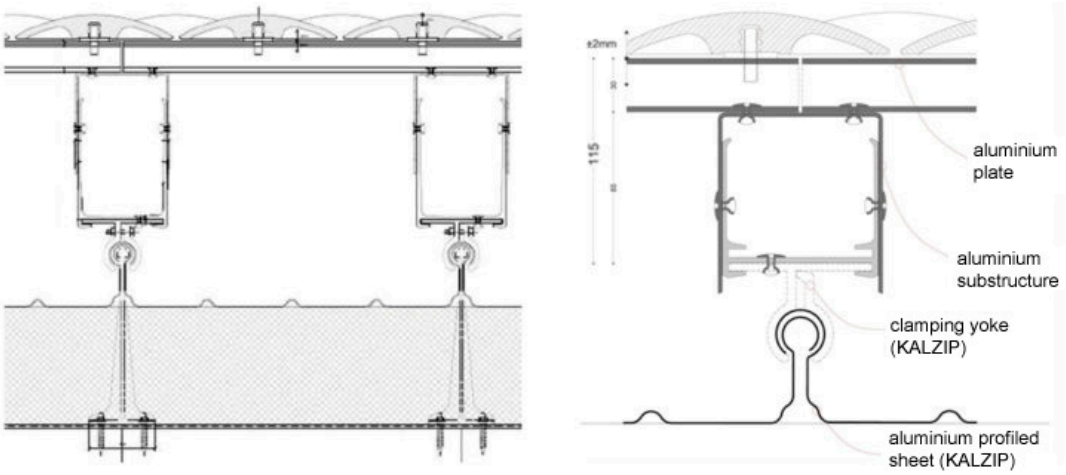

Figure 2. Construction details of the enclosure and the laying of the ceramic tiles. Tectónica. RPBW. Disset. http://tectonicablog.com/wp-content/uploads/2017/03/20-730$\times$316.jpg.

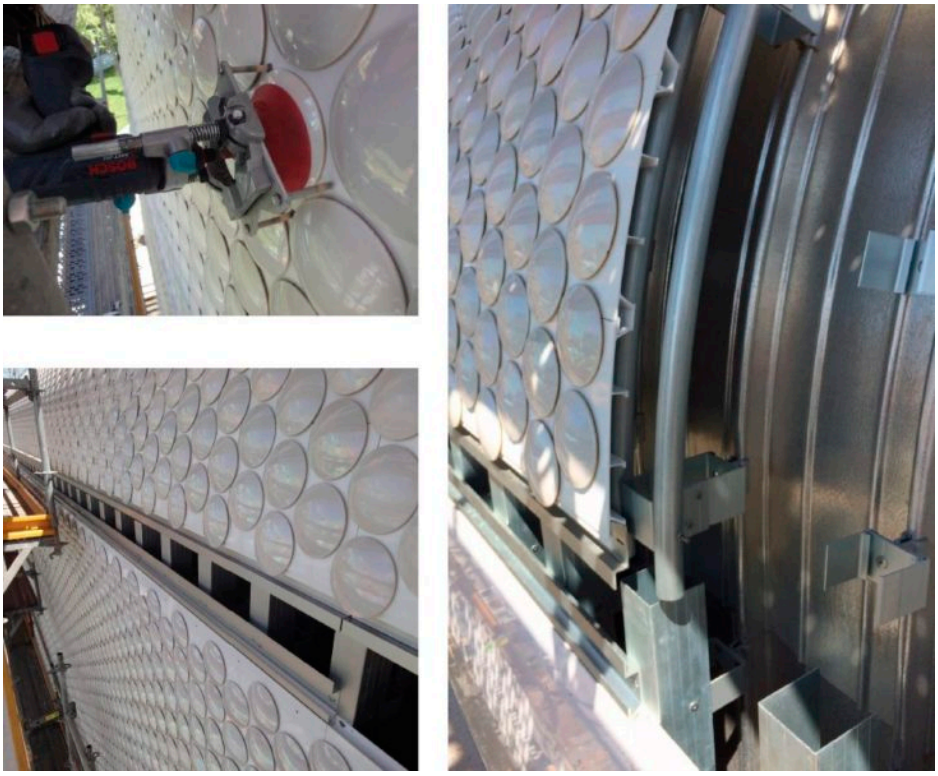

Figure 3. Ceramic tile laying system. Tectónica. RPBW. Disset. http://tectonicablog.com/wp-content/uploads/2017/03/26-730x601.jpg.

In contrast to other examples of façades in architecture where ceramics take center stage, the choice of ceramic material, and the application of existing firing, vitrification, and metal deposition techniques that give the material a pearly appearance results from a decision to avoid generating a tectonic or formal situation, and to produce only a perceptive one (Figures 4 and 5).

Figure 4. View from the roof. Chromatic integration with the sea. Photograph: Fernando Echarri.

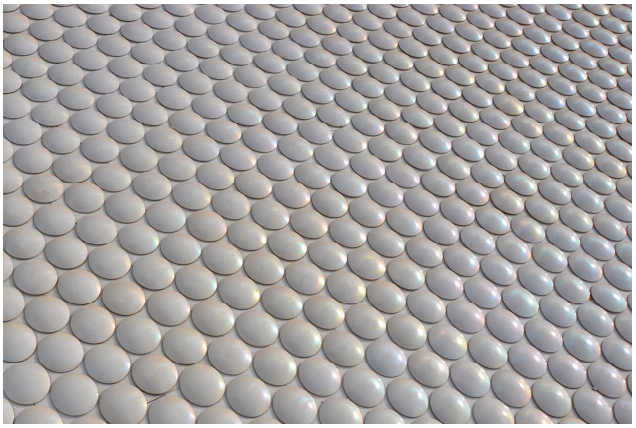

Figure 5. Ceramic tiles on the roof. Iridescent effect. Photograph: Fernando Echarri.

4. Description of the Ceramic Tile Manufacturing Process

The ceramic discs (iridescent-porcelain) used for the headquarters of the Botín Foundation consist in materials developed with ceramic pastes vitrified at high temperatures, approximately 1200 °C. The techniques described below enable to achieve the technical qualities associated with pearly-iridescent effects and the architectural quality required for particularly weather-resistant coatings.

The ceramic tiles were manufactured based on semi-handcrafted production, with some robotized steps. As we will see, the technique used for the glazed coating is based on "third-fire" metallic luster ceramics that go back to the 9th century [53]. Each of the façade cladding's circular tiles is manufactured in circular metal revolving molds in which a specific amount of stoneware is placed by casting. Subsequently, robots extract the tiles from the molds using a suction cup and polish their edges. The method is simple and facilitates automation, which allows reaching higher levels of production performance than when using other types of molding and casting techniques. Subsequently, once the tile is formed and settled, the porcelain stoneware drying phase unfolds in a continuous process dryer at a programmed temperature, to reduce humidity and to double or triple mechanical resistance, thus allowing its subsequent processing. A shiny-glossy opaque white glaze is then applied using an airbrush. This glaze, as we will see in the XRD analysis and scanning electron microscopy (SEM), is based on zirconium oxide. Later, the tiles undergo a first firing at 1240 degrees Celsius, followed

by the pearl phase, which consists in applying a nacre effect solution that produces iridescence when reflecting light. Finally, the tiles are fired a second time at 780 °C to fix the nacre to the first layer of white glaze. This second glaze contains a higher concentration of zirconium to enhance the iridescent effect (Figure 6).

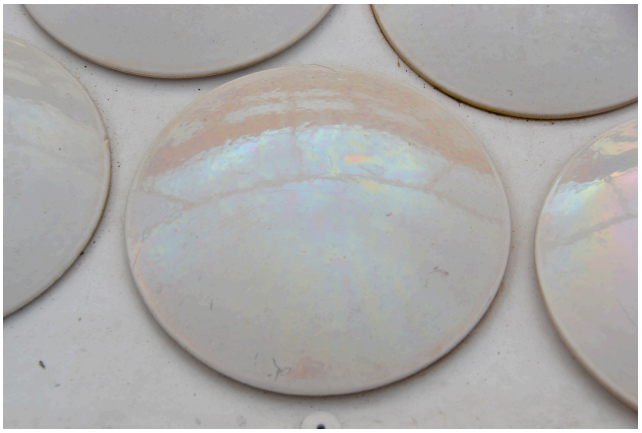

Figure 6. Enclosure ceramic tile with an iridescent and reflected light effect. Photograph: Fernando Echarri.

In other similar processes, the iridescent effect is obtained by means of three or even four firings, according to the case: the first firing is at 950 °C to obtain the biscuit, the second fires the white base glaze, and vitrifies the biscuit at 1180 °C in a fast cycle; the last firing multiplies the iridescent-pearly effect or metallic reflection between 650 °C and 780 °C—this latter firing can be either oxidation or reduction firing. It is precisely before this third firing that the balsam formed by the dissolution of metal salts in resonates [54] is applied to vitrified glazes. Recent studies have performed several eutectic combinations with satisfactory results [55–57]. The applied glaze is composed of a mixture of oxides of different metals, with particles of varying expansion coefficients, and sizes between 50 and 350 microns. Some recent studies have described iridescent and pearly effects by applying glazes containing various types of metal oxides: zinc oxide, zirconium oxide, yttrium oxide, titanium oxide, hafnium oxide and cerium oxide [58]. The application of glazes by any of the usual methods: bell-shaped system, airbrush, disc glazing, spraying, immersion, screen printing applications represent typical processes to generate iridescent ceramic. The microcracking process of some multilayer glazes has also significantly favored ceramic tile iridescence (Figure 7). The application of other techniques, such as glazing with a brush, has succeeded in enhancing the iridescent effect of the porcelain stoneware tiles [59].

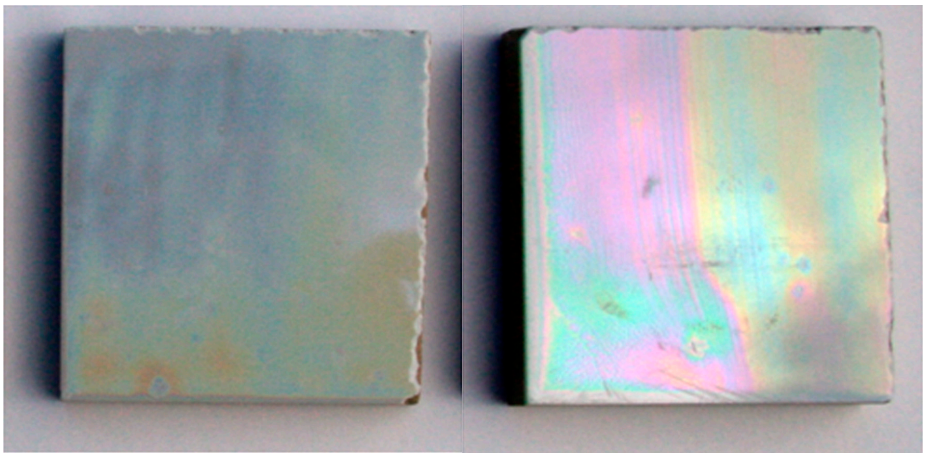

Figure 7. Samples of porcelain stoneware with zirconium oxide (ZrO_2) glaze and final glaze with anatasa (TiO_2).

5. Physical-Chemical Analysis of the Ceramic Tiles

The circular ceramic tiles' multi-layered vitrification result was characterized. To do this, XRD and SEM analyses were conducted. The XRD was performed in two phases, for angle 2θ between 25–113 and 3–70, and step 0.05.

First, a section of the tile was cut with a diamond disc. Only one glaze seemed to exist on the porcelain stoneware support, with a continuous thickness of approximately 200 microns (Figure 8). The layer of enamel can be seen in the upper section of Figure 8 shown in a lighter color. The zirconium content amounted to 4.66%, while other metals such as iron or zinc only presented a percentage of 0.14% and 1.21%, respectively. The mapping performed in the SEM microscopy allowed observing that the distribution of Zr was homogeneous as well as that of the rest of the metals (Figure 9). The distribution of Zr is shown is red, and the similarly homogeneous distribution of Zn in the layer of enamel is shown in green.

Figure 8. SEM microscope applying 150 magnifications of a tile section. Porcelain stoneware and glazed substrate.

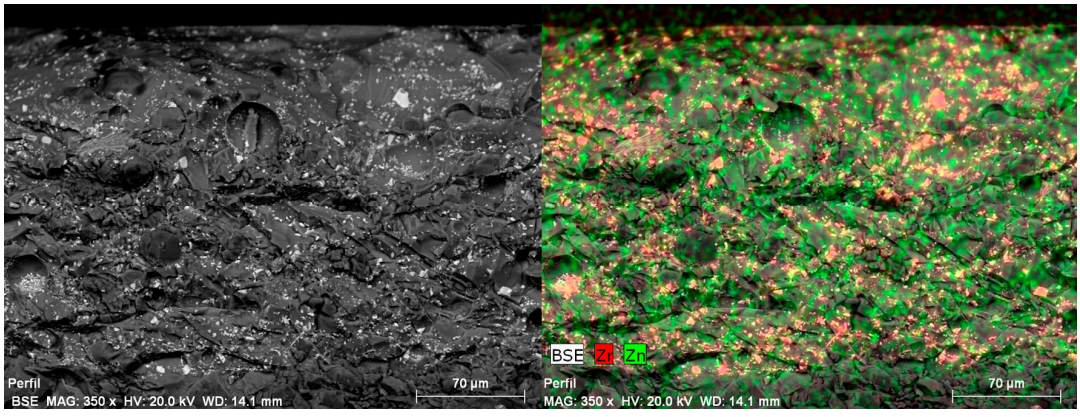

Figure 9. SEM applying 350 magnifications of the ZrO_2 glaze. Homogeneous distribution of Zr and Zn.

In Figure 10, corresponding to sample No. 1, a significant amount of zirconium was found, together with other metals such as zinc, iron and a low presence of aluminum, undoubtedly associated with the composition of the ZrO_2 zirconium oxide-based glaze. The subsequent XRD analysis determined that the presence of Zr was in the zirconium silicate Zr (SiO_4).

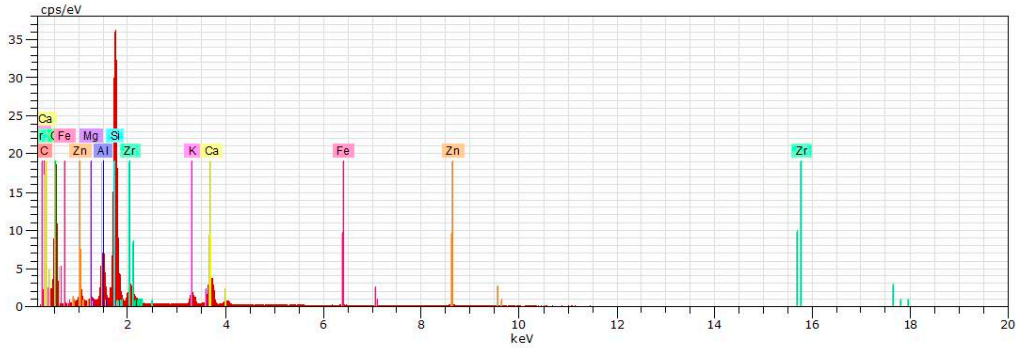

Figure 10. Energy Dispersive X-ray Spectrometer (EDS) of the section of the first layer of ZrO_2 glaze.

Secondly, the top layer of enamel on the ceramic piece was analyzed, this time not in cross section but on the surface (Figure 11). The results obtained by SEM microscopy indicated the presence of zirconium, though amounting to 9.15%, that is twice the amount detected in the previous cross section. Worthy of note, the microscope examines a thickness of around 4 microns. This led us to conclude that it corresponded to a second laying of glaze, applied with an airbrush, a few microns thick, and of similar composition, since no differentiation was observed based on the SEM in the previous tile section. Moreover, it coincided with the theoretical description of the manufacturing system used, with a second firing at 780 °C. It consisted of a ZrO_2 zirconium oxide-based glaze, but with a higher concentration than the first glaze layer. In addition, this second glaze layer produced a substantially different result compared to the first. The distribution of other metals such as zinc or titanium was homogeneous, while the distribution of zirconium was more dispersed, with distances between 30 to 50 microns between the metal's concentration nuclei. Figure 12 shows in green the homogeneous distribution of Zn, whereas on the right, Zr, shown in red, is scattered, with clusters of 50 square micrometers, and a separation of 60–80 micrometers. The crystallization of zirconium silicate favors the sunlight's diffraction effect, leading to a greater iridescent effect. This phenomenon probably causes the iridescent effect produced on the ceramic tiles' spherical outer surface, added to the fact that these discontinuities have a similar size to the wavelength of the diffracted light, as explained in Section 2.

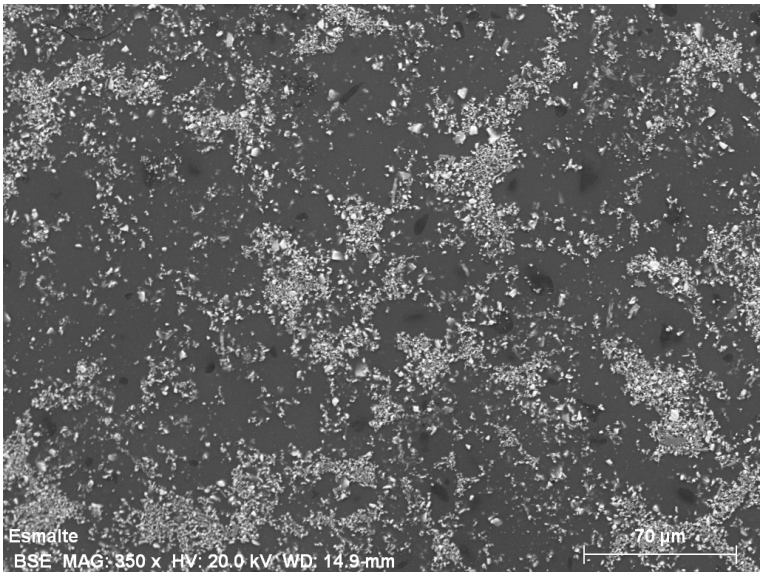

Figure 11. SEM applying 350 magnifications of the tile's second layer of glaze or final glaze.

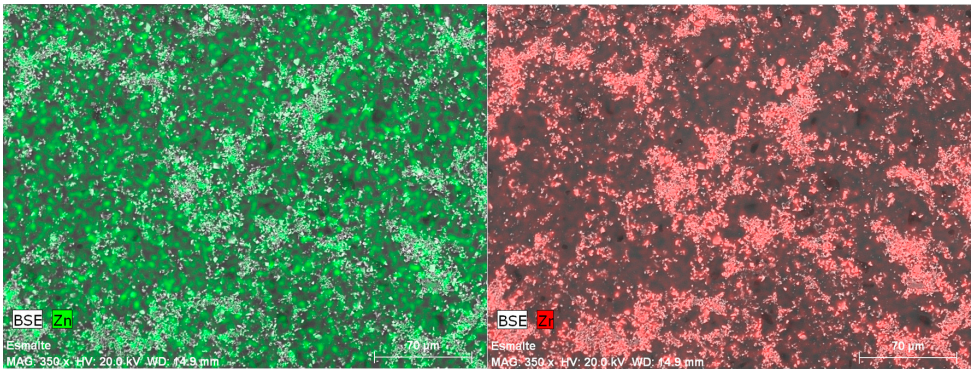

Figure 12. SEM applying 350 magnifications of the second glaze ZrO_2 layer. Distribution of Zn and Zr.

This latter dispersion of zirconium is responsible for the light diffraction phenomenon when light falls on zirconium and zinc. The physical-optical phenomenon is mainly caused by the lack of homogeneity in the distribution of Zr in the outer glaze layer. In its trajectory, light encounters different refractive indices among the Zr and Zn metals, it diffracts when reaching the zirconium silicate crystallization, also due to the relation of its wavelength with respect to the dispersion of Zr and induces white light to separate into all the colors of the spectrum. The wavelengths produced interfere with each other causing an iridescent effect.

We can launch this hypothesis based on the analysis of the glaze surface: after having conducted SEM analyses (Figure 13) applying 300 to 3000 magnifications, no microcracks were detected in the second glaze layer. We must remember that since both glazes have a similar chemical base, and though the second layer has a higher concentration of zirconium, no surface tensions took place in the cooling phase, as in the case of other ceramic tiles with multilayer glazes and a titanium oxide finishing [59]. In this case, the microcracking was due to the differences in the thermal expansion coefficients of titanium and zirconium [60] 1.3 and 0.3×10^{-5} pul/pul/°C. The microcracks phenomenon was thus dismissed as a possible cause of iridescent effects.

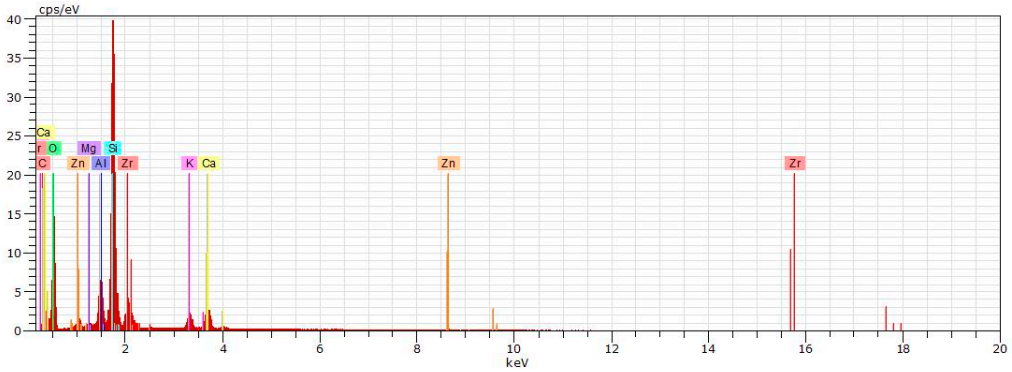

Figure 13. EDS of the second glaze layer or final glazing of ZrO_2.

We observed, by means of the XRD analysis, the presence of the following compounds in the ceramic tile's final glaze (Figure 14): zirconium silicate Zr (SiO_4), silica (SiO_2), tridymite (SiO_2), cristobalite alpha (SiO_2), cristobalite syn (SiO_2), and zirconium calcium silicate $Ca_2ZrSi_4O_{12}$.

Third, the internal face of the ceramic tile, hidden from view in the building, was analyzed (Figure 15). We observed that a discontinuous surface treatment had been applied, based on zirconium oxide ZrO_2. The presence of zirconium silicate Zr (SiO_4), silica (SiO_2) and tridymite (SiO_2) was obtained in the XRD. Figure 16 shows the homogeneous distribution of aluminum in blue, and the distribution of zinc in green, whereas the scattered presence of zirconium is shown in red. A glaze was applied to the porcelain stoneware base during the first firing using an airbrush, and this glaze was similar to the last glaze layer of the exposed face. No iridescent effect was produced as it was not applied to the

first glazing of the white base. A uniform distribution of zinc and aluminum was found according to the SEM's metal mapping, while the zirconium appeared in small circles, an effect of the zirconium oxide glaze drops. In areas where zirconium was not visible, aluminum appeared on the base of the porcelain stoneware (mullita $3Al_2O_3$-SiO_2). The presence of titanium was scant, and no anatase glazes were applied (Figure 17).

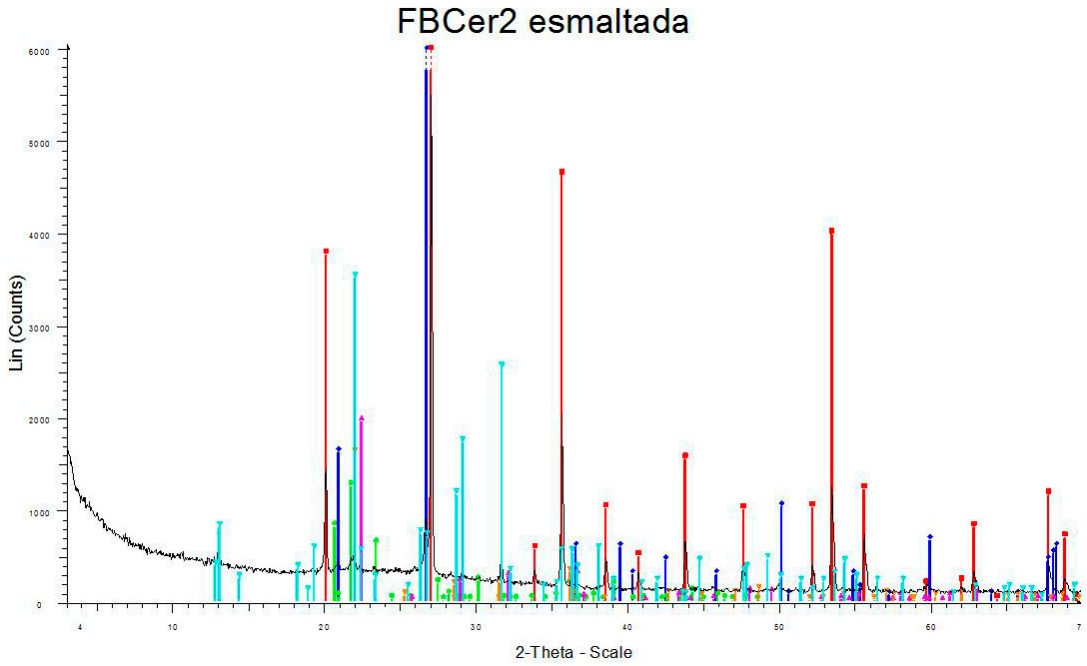

Figure 14. XRD DRX of the final layer of the ceramic tile glaze.

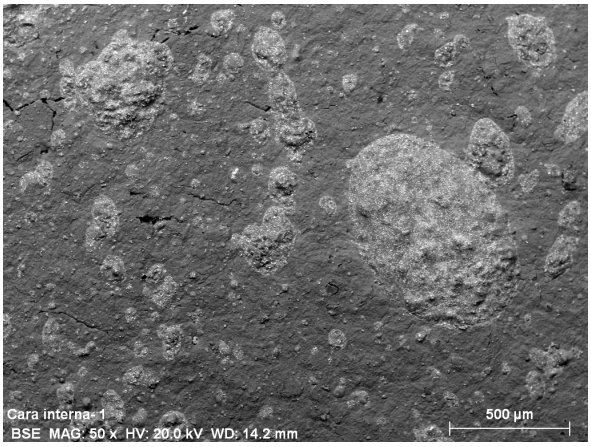

Figure 15. SEM of the ceramic tile's hidden face applying 50 magnifications.

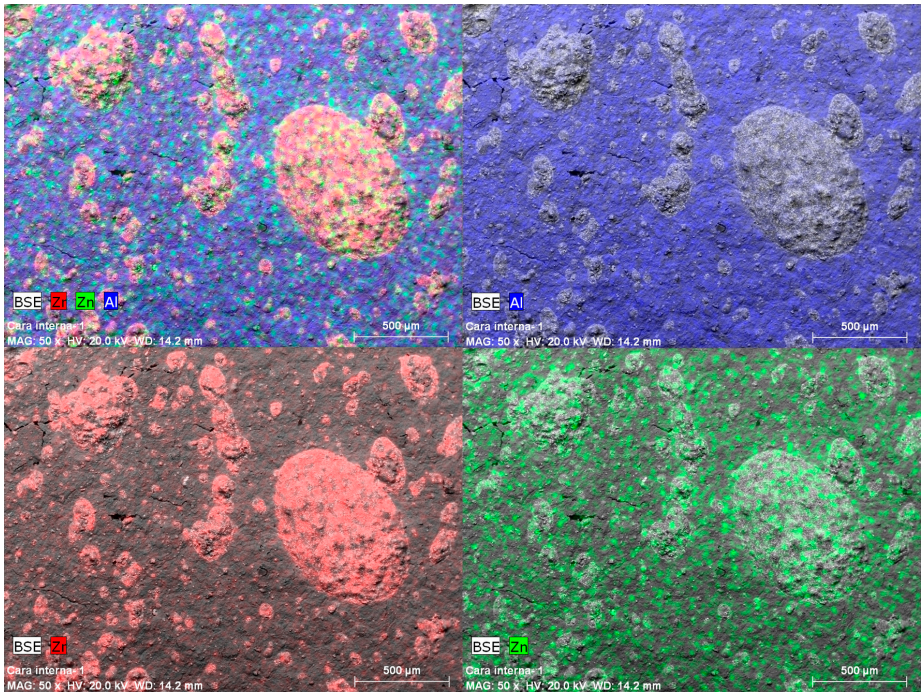

Figure 16. SEM of the ceramic tile's hidden face. Distribution of Zr, Zn, and Al.

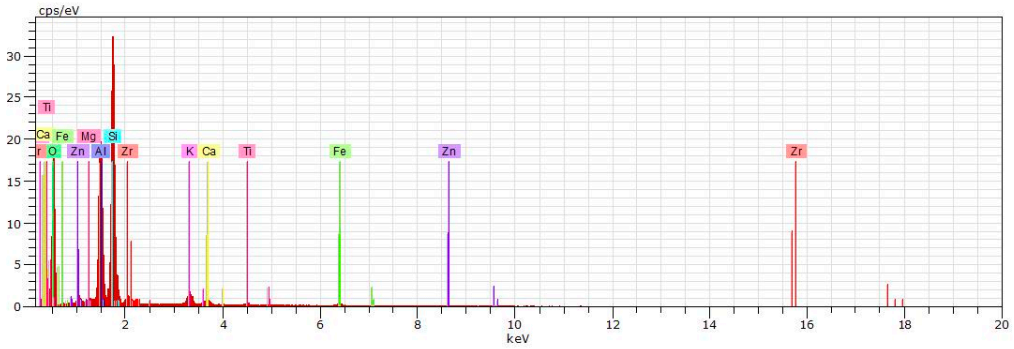

Figure 17. Energy Dispersive X-ray Spectrometer (EDS) of the ceramic tile's hidden face.

The last analyzed sample corresponded to the interior material, after having cut through it using a diamond disc. After examining the porcelain stoneware's ceramic base, the presence of silica and mullite was confirmed, with a percentage of aluminum higher than 15%, in addition to impurities such as titanium, iron, sodium, and potassium, in very low percentages (Figure 18). A lack of presence of zirconium or zinc, only present in the two layers of glazing applied, was confirmed.

Table 1 sets out the results of the element analysis or chemical characterization of the energy dispersive spectrometry (EDS) obtained for the 4 samples analyzed. In the case of the hidden face of the ceramic piece, because this is a discontinuous enamel treatment applied by airbrush, results have been shown for two measurements taken in two different areas of the SEM. Only the value "norm. C [wt.%]" is shown, which is the normalized concentration in weight per cent of each element. The presence of Zr is seen in the two enamels, with double the concentration in the top layer of enamel, and the absence of Ti and Fe in the enamels. These metals appear in the hidden face and interior section samples, along with a notable presence of aluminum.

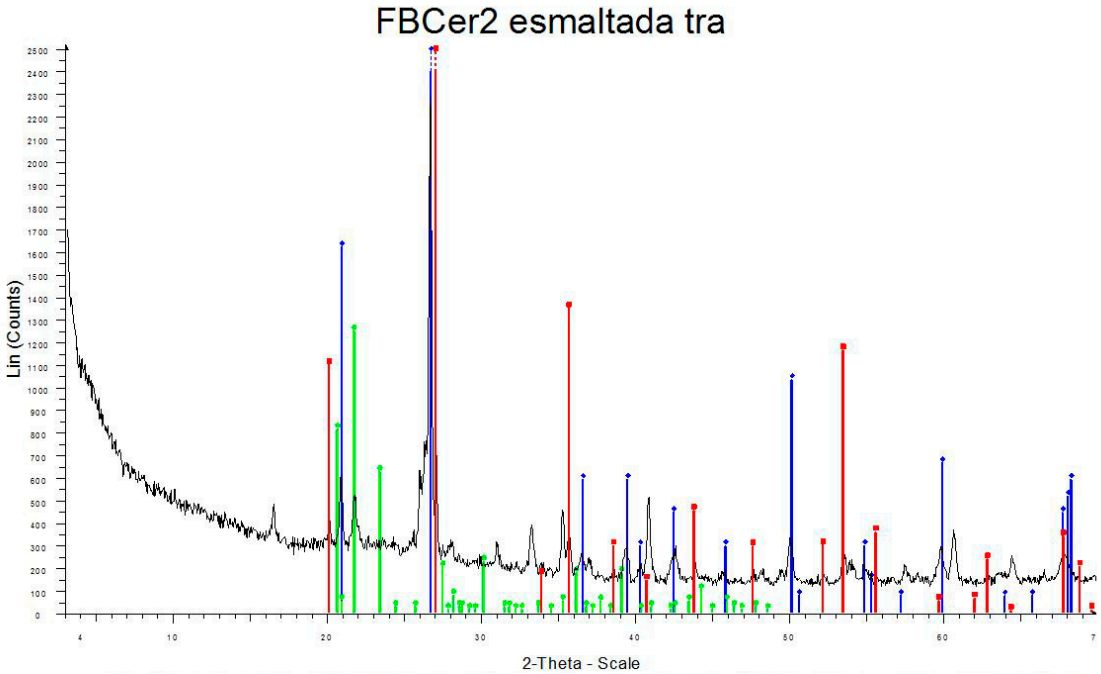

Figure 18. XRD of the ceramic tile's hidden face. Presence of zirconium silicate Zr (SiO_4), silica (SiO_2) and tridymite (SiO_2).

Table 1. Results of the presence of zirconium, zinc, titanium, iron, and aluminum in the 4 samples analyzed.

	Norm. C [wt.%]				
	SAMPLE 1 Profile	**SAMPLE 2 Glaze**	**SAMPLE 3 Hidden Face (A)**	**SAMPLE 3 Hidden Face (B)**	**SAMPLE 4 Interior**
C	14.18	4.55			
O	52.55	47.32	52.16	50.09	51.04
F				0.41	
Mg	0.63	0.30	0.55	0.56	0.99
Al	3.83	4.48	15.21	12.90	16.85
Si	16.79	25.37	24.77	25.86	27.34
K	1.36	2.73	1.99	2.11	1.74
Ca	4.79	4.37	0.76	1.41	0.25
Ti			0.50	0.40	0.64
Fe			0.97	0.88	1.15
Zn	1.21	1.02	0.13	0.38	
Zr	4.66	9.15	2.97	5.01	
TOTAL	100%	100%	100%	100%	100%

When irradiated onto the sample to be analyzed, X-rays diffract at angles that depend on interatomic distances. This non-destructive method of analysis has been used for the qualitative identification of the mineralogical composition of crystalline samples. The equipment used in the technical services of Alicante University is a Bruker D8-Advance fitted with a Göebel mirror (non-flat

samples) with a high temperature camera (up to 900 °C), and a KRISTALLOFLEX K 760–80F X-ray generator (Power: 3000 W, Voltage: 20–60 KV and Current: 5–80 mA), fitted with an X-ray tube with copper anode. The ICDD (International Center for Diffraction Data) database was used. Analysis was conducted in two stages: the first for a 2θ angular scan between 25–113 degrees, and the second between 3–70 degrees with STEP = 0.05.

SEM has enabled the identification of elements present and the establishment of their concentration. The images obtained in SEM correspond to secondary electrons or backscattered electrons emitted following interaction with the sample of an incident beam of between 5 and 30 KeV. The beam of electrons is moved around the sample, scanning in both X and Y directions. The signal from secondary electrons is formed on a thin surface layer, of between 50 and 100 Å. They are low energy electrons, less than 50 eV, which can be easily diverted from their initial emerging trajectory and allow information to be obtained about areas that are not in the sight of the detector. This peculiarity enables this signal to provide information 'in relief'. The X-rays generated in a sample subjected to electronic bombardment allow the elements present to be identified and their concentration established. The equipment used is a Hitachi model S3000N scanning electron microscope. This microscope has a Bruker model Xflash 3001 X-ray detector for microanalysis (EDS) and mapping. This SEM is fitted with an EDS capable of collecting the X-rays generated by the sample and conducting various analyses and images of the distribution of elements on polished surfaces. It has a variable pressure mode to observe non-conductive samples without having to cover them with a conductive material. The samples were prepared using an ELECTRON MICROSCOPY SCIENCES model EMS 850 critical point dryer, and a BALZERS model SCD 004 thermal sprayer (Au)/evaporator (C).

The final result of the manufacturing process is a porcelain stoneware tile whose constructive characteristics are known. It includes, however, a vitrified glaze with no microcracks, making it resistant to the actions of moisture, frost and chemicals while the goniochromatic or iridescent color characteristics that compose it are enhanced. Regarding its construction characteristics, the material is 8 to 10 mm thick, and its central part is reinforced to receive the anchorage mechanism, with a water absorption capacity of 0.1% [61] BIa group; bending strength 52 N/mm^2 [62], more than 35 N/mm^2; resistant to surface abrasion PEI V [63]; crazing resistance; frost resistance [64]; resistance to chemical agents: GHA [65]; stain resistance Class 5; friction coefficient: American Society for Testing and Materials (ASTM) fh = 0.39, ASTM fs = 0.63; resistance to thermal shock [66].

6. Colorimetric Study

We will now evaluate the goniochromatic or iridescent colors of the Botín Foundation's ceramics in Santander, resulting from the manufacturing process and curing of glazes described above. The colorimetric study was carried out using mainly a BYK-Gardner multi-angle BYK-mac model spectrophotometer (Figure 19): the device configuration allows the measurement of reflected light according to the ASTM E2194 [67] standard, typically used in goniochromatic colors [68] for the automotive sector [69], but also in cosmetics and other industrial sectors. To measure the color, the light strikes the sample at 45 degrees, and the reflected light is determined at six different angular positions—known as six different measurement geometries—as illustrated in Figure 19.

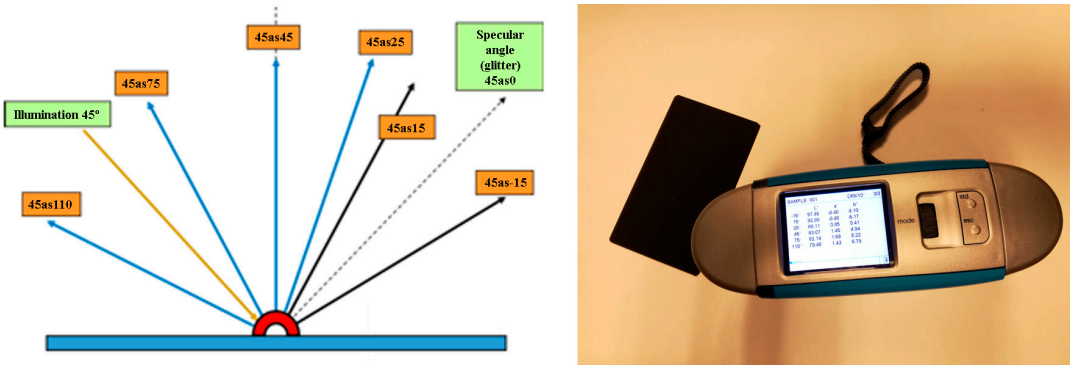

Figure 19. Measurement geometries (**left**) and multi-angle instrument used (**right**).

The spectral radiance factor, or reflectance, is determined for each measurement geometry, and the chromaticity coordinates in the CIE-L*a*b* space under the D65 illuminant (daylight) are calculated based on these factors. Figure 20 shows the sample's reflectances based on the 6 different measured geometries. Reflectance values higher than 100 are normal for this kind of materials due to the measuring conditions, employing a non-glossy white standard as reference that is less bright than the measured samples. As shown, the spectral measurements of the characteristic colors [70] appear to tilt around the spectral profile, and the geometries closest to the direction of brightness are more luminous and bluish.

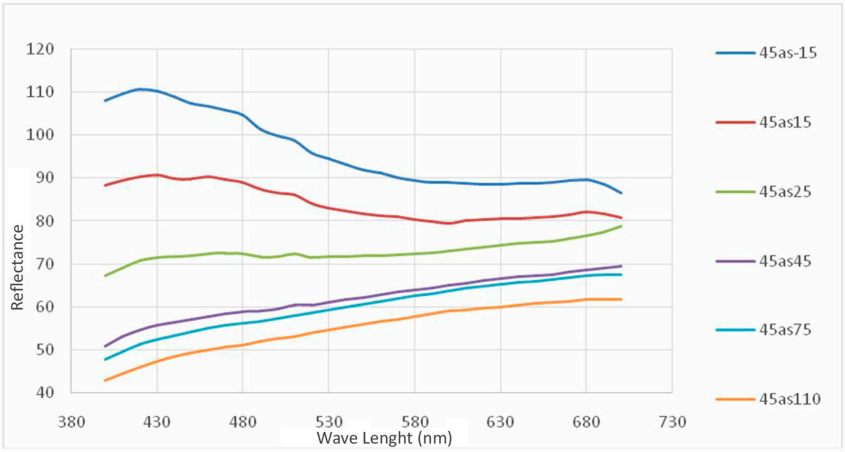

Figure 20. The sample's spectral reflectance curves for the six measurement geometries. The geometries closest to the direction of brightness are more luminous and bluish.

Figure 21 shows the tone profiles (a*,b*) and chroma/clarity. The orange point indicates the initial geometry 45as-15, and the curve marks the color change following the other five correlatively measured geometries. Color travel curves show a color change with a highly distinctive direction along the a* axis. This corresponds to a variation from a blue to a yellow hue, while the C*, L*ab profile marks a progressive color darkening at the same time.

Therefore, the sample is whitish and displays a goniochromatic behavior; both the perceived tone and the chroma/clarity of the color changes, according to the light source and the observer's position. Unlike other iridescent ceramic tiles, these tiles can offer a much broader chromatic variety observable in buildings with artificial lighting in specific positions and directions; color changes perceived in the ceramic tiles of the Botín Foundation range from a luminous bluish hue to a darker yellow one. This adds value to the initial attractiveness of this iconic building with an exceptional coastal location in the city of Santander.

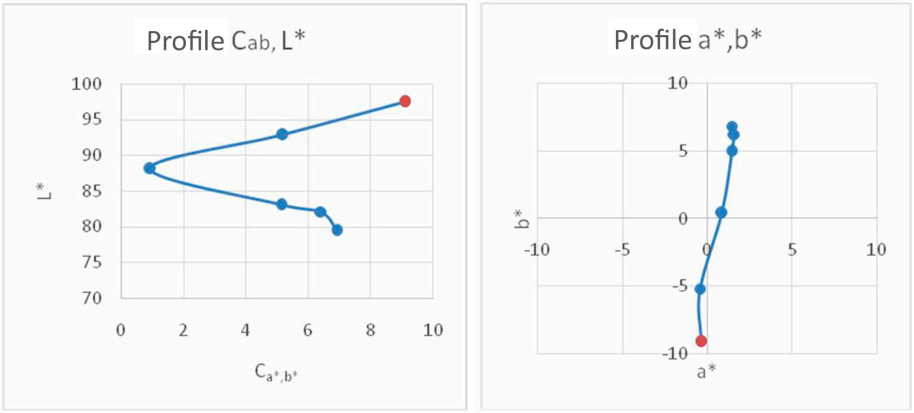

Figure 21. Tone profiles (a*,b*) and Chroma/Clarity for the six measurement geometries.

7. Conclusions

In recent years, there has been much research on new applications of ceramic materials in buildings. Porcelain stoneware, whether produced by pressing or by extrusion, has been applied in a highly versatile way to building enclosures. New-generation, large-format tiles, have opened a novel field and the possibility of ventilated façade solutions of high design quality. These new building enclosures made of porcelain tiles require no maintenance, they improve energy efficiency, and are highly durable due to low water absorption and chemical inalterability. However, little research has been conducted on color treatment and light reflection applied to this new generation of ceramic materials.

The application of glazes in ceramic tiles based on oxides of zirconium, titanium, cerium or zinc produces an iridescent and pearly effect that adds value to the enclosures. They produce new visual and perceptive effects of buildings and urban spaces for onlookers. Applying these glazes, usually in different layers, produces light reflection and refraction effects, which allows working on different color ranges depending on the glazing process. Curing these glazes' vitrification is critical to obtain iridescent and pearly results.

The ceramic tiles of the headquarters of the Botín Foundation in Santander, resemble spherical caps and two layers of glaze based on zirconium oxide were applied. The first layer, with a white base and about 200 microns thick, produces a fairly homogeneous distribution of Zr after firing that is present in 4.66% of the surface in the form of zirconium silicate Zr (SiO_4), containing a small proportion of zinc (1.21%). The second glaze layer is applied to the first layer with a second firing at 780 °C—in contrast to 1240 °C for the first glaze—and is based on zirconium oxide but with a higher metal concentration. The result, as analyzed through SEM microscopy and XRD, is a layer of a few microns with a significant presence of zirconium (9.15%) in the form of zirconium silicate Zr (SiO_4). In this case, however, the distribution of Zr is not homogeneous, displaying separate microzones of concentration between 30 and 50 microns. This latter dispersion, at the appropriate scale, produces the phenomenon of the diffraction of light when hitting zirconium and zinc. The physical-optical phenomenon is mainly caused by the distribution irregularities of Zr that the light finds in its trajectory when crossing the second layer of glazing, located on the outside, and when encountering the first layer of glazing with homogenously distributed Zr. This is how white light passes through this thin glaze layer with a different refractive index, diffracts when hitting the crystallization of zirconium silicate—also due to the relation of its wavelength to the dispersion of Zr—and induces the separation of white light into all the colors of the spectrum. The wavelengths interfere with each other causing iridescence.

The iridescent effect of the ceramic tiles analyzed is of a lower intensity than other examples of applications in buildings. In the latter, a greater number of glaze layers are usually applied using deposited metals such as Zr, Ti, Ce or Zn. A last layer of anatase (TiO_2) with a thickness between 0.5 and one micron and fired at a lower temperature is usually applied on the previous layers of glazed metal oxides. Due to differences in coefficients of thermal expansion between titanium and

zirconium, between 1.3 and 0.3×10^{-5} pul/pul/°C, a retraction occurs with resulting microcracks. This microcracking multiplies the iridescent effect and produces other chromatic ranges. In our case, the final anatase layer was not applied.

To finish, the Botín Foundation's façade presents a goniochromatic visual appeal for the spatially inhomogeneous thermal curing process of the initially pre-formulated ceramic tile. The final or characteristic colors have a slight degree of goniochromatism or metallic effect. This latter effect, however, is not as striking when observed in individual tiles of the same color. There is a notable change of direction from blue to yellow, and a simultaneous darkening of the sample. A color change is perceivable in the ceramic tiles ranging from darker bluish to a more luminous yellowish tone. The light reflection observed produces iridescent effects that help bringing the maritime environment into visitors' visual perceptions.

Author Contributions: For research articles with several authors, a short paragraph specifying their individual contributions must be Conceptualization, methodology, SEM microscopy and XRD of the ceramic samples, funding acquisition, V.E.-I.; investigation, writing—original draft preparation, V.E.-I. and A.B.G.-A.; color characterization, V.V.-P.

Funding: This research has been funded by the project "Generation of knowledge on the multisensory interaction of the human being with the environments for the development of new products and services in the ceramic sector (4 SENSES)", reference PSE-020400-2007-1, of the Ministry of Science and Innovation (Spain), of the Single Strategic Plan (2007–2009).

Acknowledgments: Our thanks to Francisco Miguel Martínez Verdú, of the University of Alicante's Vision and Color Group, http://web.ua.es/gvc. University Institute of Physics Applied to Sciences and Technologies (*IUFACyT*).

Conflicts of Interest: The authors declare no conflict of interest.

References

1. Salazar, J.; Sakamoto, T. (Eds.) *Rhythms, Cycles, Performances-Ceramics in Architecture*; ASCER; ACTAR Publishers: Barcelona, Spain, 2010; ISBN 978-8461394050.
2. Delbene, G. *Public Private Ephemeral: Ceramics in Architecture*; ASCER; ACTAR Publishers: Barcelona, Spain, 2008; ISBN 978-8461215096.
3. Norberg-Schulz, Ch. *Arquitectura Occidental*; Gustavo Gili: Barcelona, Spain, 1973; ISBN 8425218055.
4. Benevolo, L. *Storia Dell'architettura Moderna*; Editori Laterza: Bari, Italy, 1981; ISBN 9788842086222.
5. Ceramic Floor and Wall Tiles. Innovation, Avant-Garde and Sustainability in Public and Private Spaces. Report. Available online: http://www.promateriales.com/pdf/pm2209.pdf (accessed on 14 December 2018).
6. Cumella, A. Cerámics for Architecture, Granollers. Available online: http://www.cumella.cat/projectes/contemporanis/ (accessed on 16 December 2018).
7. Derby, B. Inkjet printing ceramics: From drops to solid. *J. Eur. Ceram. Soc.* **2011**, *31*, 2543–2550. [CrossRef]
8. Grespania. Technical Solutions. H&C Tiles. TiO_2 Coating That Reduces Environmental Pollution. Available online: https://www.grespania.com/baldosas-autolimpiables-anticontaminaci%C3%B3n-h&c-tiles/ref640010es (accessed on 9 January 2019).
9. Pérez-Monserrat, E.M.; Fort, R.; Lopez-Arce, P.; Alvarez de Buergo, M.; Varas-Muriel, M.J. Contribution of analytical techniques to determine the technologies used in the ceramic materials from the Former Workers Hospital of Maudes, Madrid (Spain). *J. Eur. Ceram. Soc.* **2013**, *33*, 479–491. [CrossRef]
10. Casasola, R.; Rincón, J.M.; Romero, M. Glass–ceramic glazes for ceramic tiles: A review. *J. Mater. Sci.* **2012**, *47*, 553–582. [CrossRef]
11. Pradell, T.; Pavlov, R.S.; Gutiérrez, P.C.; Climent-Font, A.; Molera, J. Composition, nanostructure, and optical properties of silver and silvercopper lusters. *J. Appl. Phys.* **2012**, *112*, 054307. [CrossRef]
12. Bobin, O.; Schvoerer, M.; Miane, J.L.; Fabre, J.F. Colored metallic shine associated to luster decoration of glazed ceramics: A theoretical analysis of the optical properties. *J. Non-Cryst. Solids* **2003**, *332*, 28–34. [CrossRef]
13. Ding, H.-Y.; Li, H.; Wang, G.-Q.; Liu, T.; Zhou, G.-H. Bio-Corrosion Behavior of Ceramic Coatings Containing Hydroxyapatite on Mg-Zn-Ca Magnesium Alloy. *Appl. Sci.* **2018**, *8*, 569. [CrossRef]
14. Zhang, Y.-N.; Lin, B.; Liu, J.-J.; Song, X.-F.; Key, J. An Experimental Study on Mechanical Modeling of Ceramics Based on Microstructure. *Appl. Sci.* **2015**, *5*, 1337–1349. [CrossRef]

15. Llusar, M.; Rodrigues, C.; Labrincha, J.; Flores, M.; Monrós, G. Reinforcement of single-firing ceramic glazes with the addition of polycrystalline tetragonal zirconia (3Y–TZP) or zircon. *J. Eur. Ceram. Soc.* **2002**, *22*, 639–652. [CrossRef]
16. Gao, Q.; Wu, X.; Fan, Y. Solar spectral optical properties of rutile TiO_2 coated mica-titania pigments. *Dyes Pigments* **2014**, *109*, 90–95. [CrossRef]
17. Yuan, L.; Han, A.; Ye, M.; Chen, X.; Ding, C.; Yao, L. Synthesis and characterization of novel non-toxic $BiFe1-_xAl_xO_3$/mica-titania pigments with high NIR reflectance. *Ceram. Int.* **2017**, *43*, 16488–16494. [CrossRef]
18. Kaya, S.Y.; Karasu, B. Process parameters determination of phosphorescent pigment added, frit-based wall tiles vetrosa decorations. *Ceram. Int.* **2012**, *38*, 2757–2766. [CrossRef]
19. Chen, T.; Zha, J.; Zhang, X.; Hu, X.; Jiang, W.; Xie, Z.; Jiang, W. Synthesis and characterization of $PrxZr1\text{-}xSiO_4$ (x = 0–0.08) yellow pigments via non-hydrolytic sol-gel method. *J. Eur. Ceram. Soc.* **2018**, *38*, 4568–4575. [CrossRef]
20. Snyders, E.; Potgieter, J.H.; Nel, J.T. The effect of milling and percentage dissociation of plasma dissociated zircon on the colour of Pr-yellow and V-blue zircon pigments. *J. Eur. Ceram. Soc.* **2006**, *26*, 1599–1603. [CrossRef]
21. Gao, Y.F.; Zhao, F.; Liu, Y.; Luo, H.J. Synthesis and characterization of ZrO_2 capsules and crystalline ZrO_2 thin layers on Fe_2O_3 powders. *CrystEngComm* **2011**, *13*, 3511–3514. [CrossRef]
22. Cavalcante, P.; Dondi, M.; Guarini, G.; Raimondo, M.; Baldi, G. Colour performance of ceramic nano-pigments. *Dyes Pigments* **2009**, *80*, 226–232. [CrossRef]
23. Jovaní, M.; Domingo, M.; Machado, T.R.; Longo, E.; Beltrán-Mir, H.; Cordoncillo, E. Pigments based on Cr and Sb doped TiO_2 prepared by microemulsionmediated solvothermal synthesis for inkjet printing on ceramics. *Dyes Pigments* **2015**, *116*, 106–113. [CrossRef]
24. Jiang, W.; Xu, X.; Chen, T.; Liu, J.; Zhang, X. Preparation and chromatic properties of $C@ZrSiO_4$ inclusion pigment via non-hydrolytic sol-gel method. *Dyes Pigments* **2015**, *114*, 55–59. [CrossRef]
25. Badenes, J.A.; Llusar, M.; Tena, M.A.; Calbo, J.; Monrós, G. Praseodymium-doped cubic $Ca–ZrO_2$ ceramic stain. *J. Eur. Ceram. Soc.* **2020**, *22*, 1981–1990. [CrossRef]
26. Ozel, E.; Turan, S. Production of coloured zircon pigments from zircon. *J. Eur. Ceram. Soc.* **2007**, *27*, 1751–1757. [CrossRef]
27. Chen, T.; Zhang, X.; Jiang, W.; Liu, J.; Jiang, W.; Xie, Z. Synthesis and application of $C@ZrSiO_4$ inclusion ceramic pigment from cotton cellulose as a colorant. *J. Eur. Ceram. Soc.* **2016**, *36*, 1811–1820. [CrossRef]
28. Colomban, P. The use of metal nanoparticles to produce yellow, red and iridescent colour, from bronze age to present times in lustre pottery and glass: Solid state chemistry, spectroscopy and nanostructure. *J. Nano Res.* **2009**, *8*, 109–132. [CrossRef]
29. Fermo, P.; Padeletti, G. The Use of Nano-Particles to Produce Iridescent Metallic Effects on Ancient Ceramic Objects. *J. Nanosci. Nanotechnol.* **2012**, *12*, 1–6. [CrossRef]
30. Barbera, G.; Barone, G.; Crupi, V.; Longo, F.; Majolino, D.; Mazzoleni, P.; Sabatino, G.; Tanasi, D.; Venuti, V. Study of Late Roman and Byzantine glass by the combined use of analytical techniques. *J. Non-Cryst. Solids* **2012**, *358*, 1554–1561. [CrossRef]
31. Garofano, I.; Robador, M.D.; Perez-Rodriguez, J.L.; Castaing, J.; Pacheco, C.; Duran, A. Ceramics from the Alcazar Palace in Seville (Spain) dated between the 11th and 15th centuries: Compositions, technological features and degradation processes. *J. Eur. Ceram. Soc.* **2015**, *35*, 4307–4319. [CrossRef]
32. Holakooei, P.; Senna, C.A.; Vasconcelos, T.L.; Archanjo, B.S.; Achete, C.A.; Abed-Esfahani, A.; Molera, J. Flashed copper and silver luster nano-structures: Characterization and technology. *Ceram. Int.* **2016**, *42*, 7757–7766. [CrossRef]
33. Roque, J.; Molera, J.; Sciau, P.; Pantos, E.; Vendrell-Saz, M. Copper and silver nanocrystals in lustre lead glazes: Development and optical properties. *J. Eur. Ceram. Soc.* **2006**, *26*, 3813–3824. [CrossRef]
34. Pradell, T.; Fernandes, R.; Molina, G.; Smith, A.D.; Molera, J.; Climent-Font, A.; Tite, M.S. Technology of production of Syrian lustre (11th to 13th century). *J. Eur. Ceram. Soc.* **2018**, *38*, 2716–2727. [CrossRef]
35. Hainschwang, T.; Notari, F. The cause of iridescence in rainbow andradite from Nara: Japan. *Gems Gemol.* **2006**, *42*, 248–258. [CrossRef]
36. Fu, J.; Peng, Y.; Tian, X. Pigments Having Angle Dependence of the Interference Colors and Its Production Process. U.S. Patent US8066811B2, 29 November 2011.

37. Tena, M.A.; Meseguer, S.; Gargori, C.; Forés, A.; Badenes, J.A.; Monrós, G. Study of Cr-SnO_2 ceramic pigment and of Ti/Sn ratio on formation and coloration of these materials. *J. Eur. Ceram. Soc.* **2007**, *27*, 215–221. [CrossRef]
38. Cannio, M.; Bondioli, F. Mechanical activation of raw materials in the synthesis of Fe_2O_3–$ZrSiO_4$ inclusion pigment. *J. Eur. Ceram. Soc.* **2012**, *32*, 643–647. [CrossRef]
39. Shen, Z.; Liu, L.; Xu, X.; Zhao, J.; Eriksson, M.; Zhong, Y.; Adolfsson, E.; Liu, Y.; Kocjan, A. Fractography of self-glazed zirconia with improved reliability. *J. Eur. Ceram. Soc.* **2017**, *37*, 4339–4345. [CrossRef]
40. Cabrera, M.J.; Montins, V.; Solsona, D.; Sala, J.M. Obtención de efectos físico-ópticos para la decoración de baldosas cerámicas. *Bol. Soc. Española Cerám. Vidrio* **2012**, *51*, IX–XVI. [CrossRef]
41. Liu, C.; Yen, M.; Han, A.; Li, J. Structural analysis and characterization of doped spinel $Co_{2-x}M_xTiO_4$ (M = Mg^{2+}, Mn^{2+}, Ni^{2+}, Cu^{2+} and Zn^{2+}) coated mica composite pigments. *Ceram. Int.* **2015**, *41*, 5537–5546. [CrossRef]
42. Jing, Ch.; Xiaobo, S.; Bing, H. The preparation and characteristics of cobalt blue colored mica titania pearlescent pigments by microemulsions. *Dyes Pigments* **2007**, *75*, 766–769. [CrossRef]
43. Bayat, N.; Baghshahi, S.; Alizadeh, P. Synthesis of white pearlescent pigments using the surface response method of statistical analysis. *Ceram. Int.* **2008**, *34*, 2029–2035. [CrossRef]
44. Ryu, Y.C.; Kim, T.G.; Seo, G.S.; Park, J.H.; Suh, C.S.; Park, S.S.; Hong, S.S.; Lee, G.D. Effect of substrate on the phase transformation of TiO_2 in pearlescent pigment. *J. Ind. Eng. Chem.* **2008**, *14*, 213–218. [CrossRef]
45. Tenório Cavalcante, P.M.; Dondi, M.; Guarini, G.; Barros, F.M.; Da Luz, A.B. Ceramic application of mica titania pearlescent pigments. *Dyes Pigments* **2007**, *74*, 1–7. [CrossRef]
46. Bertaux, S.; Reynders, P.; Heintz, J.M. Sintering of nanocrystalline Ta2O5 and ZrO_2 films compared to that of TiO_2 films. *J. Eur. Ceram. Soc.* **2006**, *26*, 923–932. [CrossRef]
47. Siligardi, C.; Montecchi, M.; Montorsi, M.; Pasquali, L. Ceria-Containing Frit for Luster in Modern Ceramic Glaze. *J. Am. Ceram. Soc.* **2010**, *93*, 2545–2550. [CrossRef]
48. Gualtieri, A.F.; Canovi, L.; Viani, A.; Bertocchi, P.; Corradini, C.; Lassinantti Gualtieri, M.; Gazzadi, G.C.; Zapparoli, M.; Berthierf, S. Mechanism of lustre formation in scheelite-based glazes. *J. Eur. Ceram. Soc.* **2013**, *33*, 2055–2064. [CrossRef]
49. Dondi, M.; Zanelli, C.; Ardit, M.; Cruciani, G.; Mantovani, L.; Tribaudino, M.; Andreozzi, G.B. Ni-free, black ceramic pigments based on Co—Cr—Fe—Mn spinels: A reappraisal of crystal structure, colour and technological behaviour. *Ceram. Int.* **2013**, *39*, 9533–9547. [CrossRef]
50. He, X.; Wang, F.; Liu, H.; Niu, L.; Wang, X. Synthesis and color properties of the TiO_2@$CoAl_2O_4$ blue pigments with low cobalt content applied in ceramic glaze. *J. Am. Ceram. Soc.* **2018**, *101*, 2578–2588. [CrossRef]
51. Chen, S.; Cheng, M.; Lang, Y.; Wei, H.; Wang, C. Synthesis and chromatic properties of zircon encapsulated ceramic black pigment with carbon sphere as carbon source. *J. Eur. Ceram. Soc.* **2018**, *38*, 2218–2227. [CrossRef]
52. Romero, M.; Rincón, J.M. Surface and Bulk Crystallization of Glass-Ceramic in the Na_2O–CaO–ZnO–PbO–Fe_2O_3–Al_2O_3–SiO_2 System Derived from a Goethite Waste. *J. Am. Ceram. Soc.* **1999**, *82*, 1313–1317. [CrossRef]
53. Colomban, P. Secrets retrouvés du Lustre Abbasside. *Rev. Céram. Verre* **2004**, *139*, 13–19.
54. Nebot-Díaz, I. *Nuevas Tecnologías para el Sector Cerámico de Castellón: Desarrollo de Esmaltes Vitrocristalinos y Vitrocerámicos*; Universitat Jaume I: Castellón, Spain, 2001.
55. Pastor, J.Y.; Poza, P.; LLorca, J.; Peña, J.I.; Merino, R.I.; Orera, V.M. Mechanical properties of directionally solidified Al_2O_3–$ZrO_2(Y_2O_3)$ eutectics. *Mater. Sci. Eng.* **2001**, *308*, 241–249. [CrossRef]
56. Peña, J.I.; Merino, R.I.; de la Fuente, G.F.; Orera, V.M. Aligned ZrO_2(c)-$CaZrO_3$ eutectics grown by the laser floating zone method: Electrical and optical properties. *Adv. Mater.* **1996**, *8*, 909–912. [CrossRef]
57. Merino, R.I. Cerámicas eutécticas solidificadas direccionalmente para fotónica y electrocerámica. *Rev. Real Acad. Cienc.* **2006**, *61*, 47–86.
58. Montins Nebot, V.; Cabrera Ibáñez, M.J.; Solsona Monzonis, D.; Sala Iniesta, J.M. Petitioner: Vidres S.A. Coating for Ceramic Bodies. Patent Application nº. 201230096, 29 July 2013.
59. Vielhaber, L. *Tecnología de los Esmaltes*; Editorial Reverté: Barcelona, Spain, 1961.
60. Echarri Iribarren, V.; González Avilés, A.B.; Ródenas, M.; Olivares, J. Cerámica y vibración de la luz. Nuevas técnicas de nacarado e irisado y caracterización colorimétrica. *Inform. Constr.* **2016**, *68*, 5–67. [CrossRef]

61. AENOR-CEN. *UNE-EN ISO 10545-3 <0.5%. Baldosas Cerámicas. Parte 3: Determinación de la Absorción de Agua, de la Porosidad Abierta, de la Densidad Relativa Aparente, y de la Densidad Aparente*; ISO 10545-3:1995, Incluye CORRIGENDUM Técnico 1:1997; Asociación Española de Normalización (AENOR): Madrid, Spain, 1997.
62. AENOR-CEN. *UNE-EN ISO 10545-4. Baldosas Cerámicas. Parte 4: Determinación de la Resistencia a la Flexión y de la Fuerza de Rotura*; ISO 10545-4:2004; Asociación Española de Normalización (AENOR): Madrid, Spain, 2009.
63. AENOR-CEN. *UNE-EN ISO 10545-7. Baldosas Cerámicas. Parte 7: Determinación de la Resistencia a la Abrasión Superficial de las Baldosas Esmaltadas*; ISO 10545-7:1996; Asociación Española de Normalización (AENOR): Madrid, Spain, 1999.
64. AENOR-CEN. *UNE-EN ISO 10545-12. Baldosas Cerámicas. Parte 12: DETERMINACIÓN de la Resistencia a la Helada*; ISO 10545-12:1995, Incluye Corrigendum Técnico 1:1997; Asociación Española de Normalización (AENOR): Madrid, Spain, 1997.
65. AENOR-CEN. *UNE-EN ISO 10545-13. Baldosas Cerámicas. Parte 13: Determinación de la Resistencia Química*; ISO 10545-13:1995; Asociación Española de Normalización (AENOR): Madrid, Spain, 1998.
66. AENOR-CEN. *ISO 10545-9. Baldosas Cerámicas. Parte 9: Determinación de la Resistencia al Choque Térmico*; ISO 10545-9:1994; Asociación Española de Normalización (AENOR): Madrid, Spain, 1997.
67. *ASTM E2194-14, Standard Test Method for Multiangle Color Measurement of Metal Flake Pigmented Materials*; ASTM International: West Conshohocken, PA, USA, 2014.
68. Klein, G.A. *Industrial Color Physics*; Springer: New York, NY, USA, 2010.
69. Chorro, E.; Perales, E.; Burgos, F.J.; Gómez, O.; Vilaseca, M.; Viqueira, V.; Pujol, J.; Martínez-Verdú, F.M. The minimum number of measurements for colour, sparkle, and graininess characterisation in gonio-apparent panels. *Color. Technol.* **2015**, *131*, 303–309. [CrossRef]
70. Ferrero, A.; Perales, E.; Rabal, A.; Campos, J.; Martínez-Verdú, F.M.; Chorro, E.; Pons, A. Color representation and interpretation of special effect coatings. *J. Opt. Soc. Am.* **2014**, *32*, 436–447. [CrossRef]